

Recent Progress in Light-Scattering Porous Polymers and Their Applications

Shudong Yu,* Junchi Chen, Guillaume Gomard, Hendrik Hölscher, and Uli Lemmer*

Conventional inorganic-nanoparticles-based scattering systems have dominated many practical applications for years. In contrast, the rise of porous polymers is perceived as a game-changer due to their low cost, facile preparation, and great abundance. One challenging issue to be tackled is the design and fabrication of porous polymers with light-scattering properties comparable to those of inorganic nanoparticles. Taking inspiration from nature (e.g., from white beetles *Cyphochilus*), scientists have achieved remarkable progress in the field of light-scattering porous polymers and their related applications in recent years. Therefore, here, an up-to-date review about this emerging field is provided. This overview covers materials for making porous polymer structures, detailed fabrication methods, and applications benefitting from their tailorable light-scattering properties. It is envisioned that more bioinspired light-scattering porous polymers will be made to be potential alternatives of conventional nanoparticles-based scatterers.

1. Introduction

Light scattering is a ubiquitous optical phenomenon occurring in the systems with refractive index inhomogeneity, such as fog, milk, and clouds, et al.^[1–3] Typically, such bulk systems contain numerous scattering particles that can deflect impinging light to randomize its direction, endowing the systems with translucency or even opacity (i.e., whiteness).^[4–6] To achieve efficient light-scattering in engineered materials, high refractive index nanoparticles are usually embedded in low refractive index matrices (e.g., resin) to create a substantial refractive index contrast. Titanium dioxide (TiO₂) nanoparticles are the most commonly adopted ones since TiO₂ features a relatively high refractive index ($n \approx 2.6$) and little absorption in the visible spectrum.^[4]

However, recent research has shown that TiO₂ nanoparticles might harm human health due to pulmonary inflammation effects and potential toxicity.^[7] In addition, doping nanoparticles into matrixes takes additional costs. Furthermore, the realization of large areas with homogeneous optical properties is difficult because potential imperfect mixing is usually inevitable. Therefore, seeking alternatives to TiO₂ nanoparticles-based systems is essential and meaningful in terms of optical performance, environmental and health point-of-view. Recently, light-scattering porous polymer structures have been revisited and pursued as alternatives to conventional nanoparticles-based scattering films, although the refractive indexes of most polymers are fairly small ($n \approx 1.4–1.6$).


Indeed, nature provides numerous brilliant scattering systems made of biopolymers, serving as excellent inspirations.^[3] As shown in **Figure 1**, one of the prominent example are the white beetles of the genus *Cyphochilus* spp., whose scales have been regarded as the best scattering biological surface ever found.^[8] The white beetle scale can reflect $\approx 70\%$ of visible light at a thickness of only $\approx 7 \mu\text{m}$, indicating that its scattering ability exceeds many artificial scattering systems (e.g., paper, photonic glass).^[9] In terms of optical transport mean free path l_t (average distance travelled by light across the sample before the direction of its propagation is randomized), its value was measured to be as low as $\approx 1.5 \mu\text{m}$. Note that the main component of the white beetle scale is chitin with a low refractive index of about 1.56. Therefore, it is no surprise that the unique porous fibril structure of the beetle scale underpins its exceptional scattering ability. It features evolutionary-optimized fibril diameter, filling fraction, scattering center distance, and a certain degree of anisotropy

S. Yu
School of Advanced Manufacturing
Sun Yat-sen University
Gongchang Road 66, Shenzhen 518107, China
E-mail: yushd6@mail.sysu.edu.cn

J. Chen, U. Lemmer
Light Technology Institute
Karlsruhe Institute of Technology (KIT)
Engesserstrasse 13, 76131 Karlsruhe, Germany
E-mail: uli.lemmer@kit.edu

G. Gomard
Carl Zeiss AG
Zeiss Innovation Hub
Hermann-von-Helmholtz-Platz 6, 76344 Eggenstein-Leopoldshafen,
Germany

H. Hölscher, U. Lemmer
Institute for Microstructure Technology
Karlsruhe Institute of Technology (KIT)
Hermann-von-Helmholtz-Platz 1, 76344 Eggenstein-Leopoldshafen, Ger-
many

 The ORCID identification number(s) for the author(s) of this article can be found under <https://doi.org/10.1002/adom.202203134>

© 2023 The Authors. Advanced Optical Materials published by Wiley-VCH GmbH. This is an open access article under the terms of the Creative Commons Attribution-NonCommercial License, which permits use, distribution and reproduction in any medium, provided the original work is properly cited and is not used for commercial purposes.

DOI: 10.1002/adom.202203134

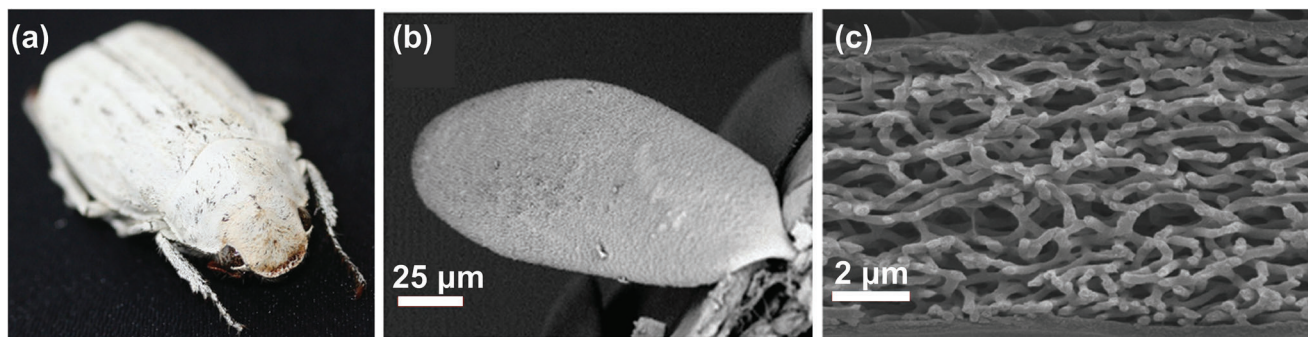


Figure 1. a) Image of white beetle *Cyphochilus*. b) Scanning electron microscopy (SEM) image of a complete scale. c) Cross-sectional SEM image of a porous scale. Reproduced with permission.^[14] Copyright 2015, The Authors, published by Wiley-VCH.

of porous network at minimum material use.^[10–16] It is discovered that diffusely incident light on the beetle scales is preferentially channeled sideways and scattered backward on the average after traversing a vertical distance corresponding to only two scattering event.^[17] The bioinspired fabrication of artificial light-scattering porous polymers with remarkable scattering performance has been largely stimulated by this natural prototype. These porous materials show great potential as alternatives to replace conventional inorganic nanoparticles.^[18] Recently, Utel et al. have demonstrated that their delicate engineered porous structure generated by a random walk algorithm possessed a larger broadband reflectance than the beetle scale at an even less material use, providing an intriguing and new insight into the design of light-scattering porous structures.^[19] The porous structure of the white beetles is not optimized for sole light-scattering properties, but rather results from a trade-off between achieving whiteness, mechanical robustness etc. In that sense it is not totally unexpected that engineered optical materials can overcome its I_r . This finding is in an agreement with previous publications, in which researchers succeeded in fabricating artificial porous polymers with stronger scattering abilities than the white beetle scale.^[20,21]

We note that researchers have become increasingly interested in the topics related to light-scattering porous polymers and their relevant applications. On the one hand, an increasing number of insects and plants with white appearance have been investigated thoroughly, including silver ants,^[22] butterflies (e.g., *Carystoides escalantei*, *Curetis acuta* Moore, *Dione vanillae*),^[23–25] beetles (e.g., *Goliathus goliatus*),^[26] and plant leaves (e.g., *Populus alba*, *Boehmeria nivea*).^[27,28] Recently, it has been demonstrated that some of the white biological surfaces can reflect solar light efficiently while radiating mid-infrared emission toward outside environment simultaneously, realizing effective daytime passive radiative cooling effects, which might be crucial to the living of those insects and plants in hot environments.^[22,26,28–30] For example, the Saharan silver ants, *Cataglyphis bombycin*, are densely covered with triangular-shaped hollow hairs on their bodies, which enable their living in an extremely hot environment with two thermoregulatory effects (i.e., solar reflection and blackbody radiation).^[22] On the other hand, inspired by the natural white layers (e.g., *Cyphochilus* scale), researchers have endeavored to develop various fabrication methods to mimic the porous structures of highly scattering white surfaces in nature.^[18,31,32] New ap-

plications enabled by those artificial light-scattering porous polymers are also developed. Due to the fast development of light-scattering porous polymers, we report in this article about the recent progress in this field and give new insights into biomimetic porous polymers. As shown in **Figure 2**, this review is outlined as follows: first, materials for making light-scattering porous polymers are introduced; second, possible fabrication methods are described; third, relevant application scenarios are presented; at last, we give some perspectives to motivate more researchers to be engaged in this rapidly developing research field.

2. Selection of Materials for Making Light-Scattering Porous Polymers

Two main types of polymers can serve as a basis for producing light-scattering porous materials: Petroleum-based polymers and biopolymers. The former polymer material is called “artificial synthetic polymer,” while the latter is directly derived from nature. Unlike many inorganic materials, most organic polymers possess a low refractive index ranging from 1.4 to 1.6, leading to a moderate scattering efficiency upon introduction of a porous network.^[39] One promising characteristic of numerous polymers is that they possess a low absorption over the visible spectrum, which is conducive to making light-scattering porous structures. Polymers can be amorphous or semi-crystalline, depending on the molecular alignment. Amorphous polymers are intrinsically transparent due to their random distribution of polymer chains. In contrast, semi-crystalline polymers appear translucent or opaque, stemming from the light scattering effect caused by the different refractive index between crystalline and amorphous regions.^[40] To enable the practicality of optical polymers, transparency is usually a prerequisite for many conventional optical applications, such as optical fibers, optical lenses, and encapsulation media, just to name a few. Therefore, the use of optical polymers for such applications is restricted to some amorphous polymers with bulk optical homogeneity, including polymethyl methacrylate (PMMA), polyurethane (PU), polycarbonate (PC), polystyrene (PS), and urethane-acrylate.^[41] The raw materials for making porous polymers cover a wider range since the intrinsic light-scattering property is not a detrimental factor in this regime. Therefore, we can see the diversity of materials used for fabricating porous polymers, which includes, but are not limited to, poly(vinylidene fluoride) (PVDF), polyethylene (PE),

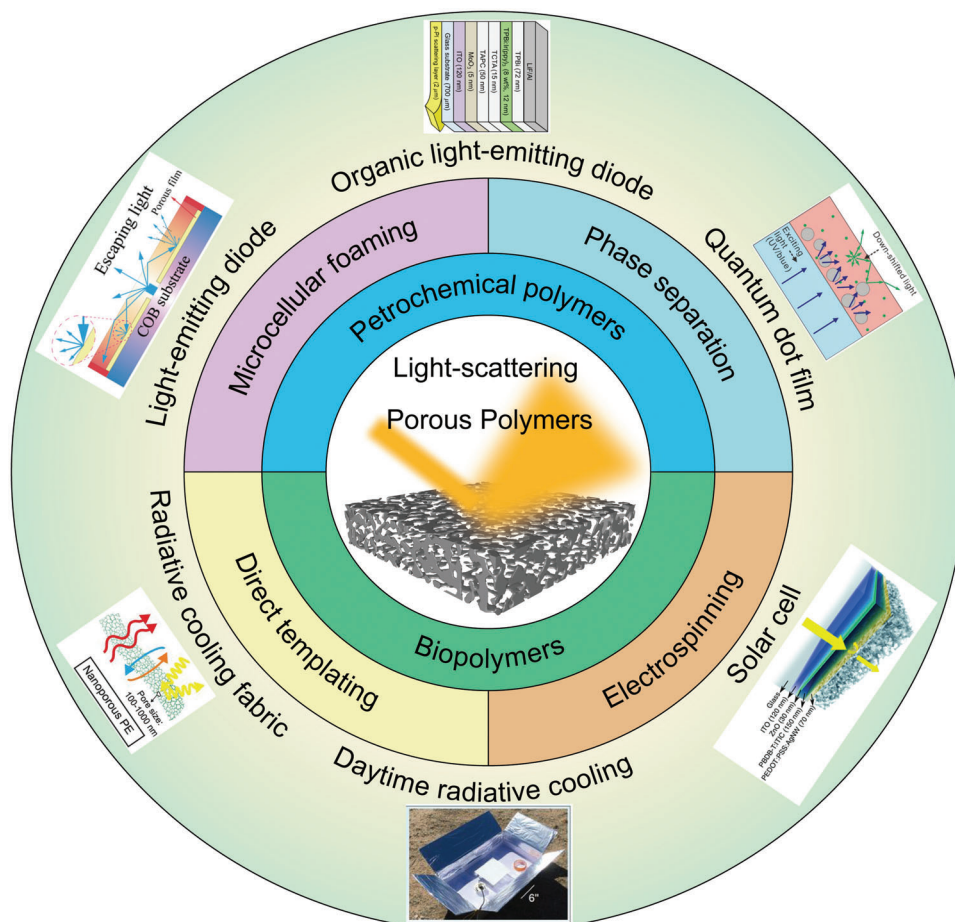


Figure 2. Schematic illustration of the structure of this review: Materials, fabrication methods for light-scattering porous polymers, and their optical and thermal applications. Porous polymer films are used as diffuse reflectors for out-coupling total internally reflected light trapped inside the light-emitting diodes (LEDs). Reproduced with permission.^[33] Copyright 2021, Wiley-VCH. The substrate mode of organic LEDs can be extracted to the free space by thin-film porous polymers. Reproduced with permission.^[34] Copyright 2015, American Chemical Society. By introducing air pores inside the quantum dot film, the photoluminescence efficiency can be largely enhanced due to the synergistic improvement effects of excitation light absorption and emission light extraction. Reproduced with permission.^[35] Copyright 2019, Wiley-VCH. As an alternative to common metallic reflectors, reflective porous polymers can be integrated onto the rear side of solar cells, enabling enhancement of power conversion efficiency by recycling transmissive light. Reproduced with permission.^[36] Copyright 2021, The Authors, published by Wiley-VCH. Porous polymers are also excellent candidates applied in the passive daytime radiative cooling^[37] and radiative cooling fabrics.^[38] Reproduced with permission.^[37] Copyright 2018, American Association for the Advancement of Science. Reproduced with permission.^[38] Copyright 2016, American Association for the Advancement of Science.

polydimethylsiloxane (PDMS). These petroleum-based polymers can be synthesized via selecting different petrochemical monomers to generate homopolymers or copolymers in a facile and cost-effective way.^[42]

Nevertheless, the lack of biodegradability for petroleum-based polymers is detrimental to the environment, which calls for biodegradable alternatives, namely biopolymers. Those typical biopolymers that can be used for optical applications include, for example, cellulose and silk. They are typically processed as fibrils with nano- and micro-scale dimensions.^[32] The cellulose is composed of glucose units, while the silk is made up of amino acid units. Both cellulose and silk feature little absorption in the visible spectrum, which is desired for making light-scattering porous structures.^[18] Cellulose is well known as the main ingredient of paper, with medium whiteness caused by the microscale dimension of cellulose fibrils.^[43] With a size in the nanoscale

range, cellulose nanofibrils can be cast into porous structures with extreme whiteness.^[44] Intriguingly, cellulose nanofibrils can also be used to fabricate highly transmissive paper either with large haze or good transparency. This property might enable numerous applications in optoelectronics (e.g., solar cells; organic LEDs, OLEDs) for advanced light management.^[45–49] Native silk fibers are intrinsically arranged into delicate porous structures with brilliant whiteness stemming from the unique Anderson light localization in the silk nanofibril matrix.^[50] The scattering effect is caused by numerous densely packed parallel fibrillar nanopores packing together along the longitudinal axis. Such a strong scattering scheme arising from silk nanofibrils can be further enhanced by reconstructing a native silk film into a fibrous film with a mean fiber diameter of 250 nm via electrospinning.^[51] The results also highlight the importance of structure tailoring to produce highly scattering porous media from pristine

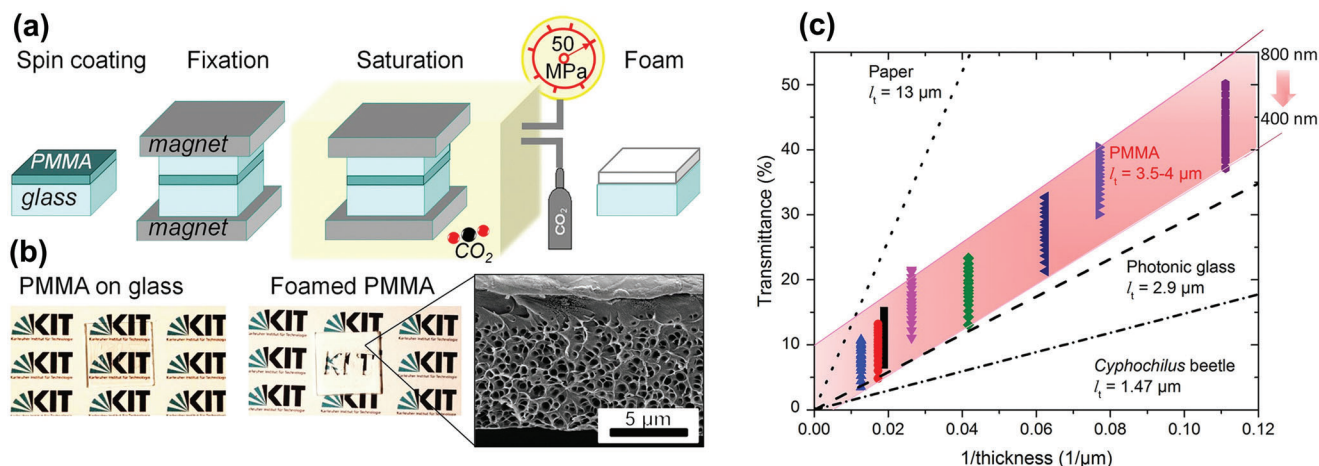


Figure 3. a) Schematic diagram of microcellular foaming process based on supercritical CO_2 . b) Left: Transparent PMMA film on the glass; Right: Foamed PMMA with a brilliant whiteness and its cross-sectional nanoporous morphology. c) Plot of transmittance of foamed PMMA films versus their corresponding inverse of thickness, deriving a mean free optical path l_t of 3.5–4 μm in the range 400–800 nm. Reproduced with permission.^[7] Copyright 2017, The Authors, published by Springer Nature.

materials with moderate scattering abilities. Nature possesses abundant biopolymers that could be harnessed to make light-scattering porous structures, which deserves further exploitation.

3. Fabrication Methods for Making Light-Scattering Porous Polymers

3.1. Microcellular Foaming

Microcellular foaming is a versatile and facile technique that has been utilized to fabricate porous polymers with enhanced thermal insulation and impact-resistant mechanical properties.^[52] To fabricate light-scattering nano-porous polymers via microcellular foaming, careful attention is needed since this method usually generates macro-porous structures with pore sizes ranging from tens to hundreds of micrometers. This is advantageous for improving thermal and mechanical properties of foamed materials, but light scattering is not pronounced for such large pore sizes. Since our interest is in the visible and near-infrared spectra, the target pore size of porous polymers should fall into the range of hundreds of nanometers to several micrometers to maximize the scattering efficiency of the pores.^[37]

These guidelines are also applicable to microcellular foaming using non-toxic carbon dioxide (CO_2) as a physical blowing agent. This approach has been attracting increasing attention from both, academia as well as industry, and can also be adopted for fabricating light-scattering porous polymers. As shown in **Figure 3a**, Syurik et al. demonstrated the feasibility of microcellular foaming based on CO_2 for making highly scattering films.^[7] The foaming process contains four main steps: i) CO_2 dissolution into the polymer matrix at elevated pressure and temperature to form an equilibrium polymer- CO_2 system till saturation; ii) pore nucleation by subjecting the polymer- CO_2 system into supersaturation state by increasing temperature or pressure quenching; iii) pore growth driven by the temperature difference between the applied temperature T and the glass transition temperature T_g ($T > T_g$); iv) pore growth is terminated and frozen into fixed morphology

when $T < T_g$. Since the CO_2 -absorption capability depends on the type of polymer considered, the foamed polymers have a great influence on the ultimate porous network. Apart from material parameters, processing conditions including foaming pressure and temperature, are also critical to control of the attained porous morphology of the polymers. It was shown that a larger foaming pressure leads to a reduced pore size, which is recommended to be larger than 30 MPa due to the resultant optimal whiteness. In addition, a several-micrometers-thick skin layer without pores (see the SEM image in **Figure 3b**) appears at the film/air interface, caused by the spontaneous diffusion of CO_2 toward free space after the pressure quenching operation. Note that increasing foaming pressure can effectively reduce the thickness of the skin layer. Therefore, it is rational to use a large foaming pressure for processing thin polymer layers since the skin layer makes no contributions to the ultimate scattering performance. It is well noted that increasing the foaming temperature causes both the growth of pore size and the filling fraction of pores. Finally, the most brilliant whiteness of the foamed polymer (here PMMA) was realized at 50 MPa and 80 °C, featuring a nanoporous morphology with an average pore diameter of ≈ 300 nm and a porosity of $\approx 40\%$ (see **Figure 3b**) and l_t values ranging from 3.5 to 4 μm in the visible range of 400–800 nm (see **Figure 3c**). Specifically, a 9 μm -thick scattering layer features a reflectance above 57%, indicating its excellent scattering performance endowed by the nanoporous network. Note that the ultrahigh molecular weight of PMMA ($M_w = 950$ K) also plays an important role in generating the nanoscale pores since using the same parameters for foaming low-molecular-weight PMMA ($M_w = 15$ K) only leads to microscale pores with a pore diameter larger than 1 μm .^[35] The underlying mechanism can be well explained by the fact that the exclusion of the low-molecular-weight part in polymers is conducive to the onset of heterogeneous nucleation. This, in turn, tends to produce an ultrahigh density of pores with reduced pore sizes.^[53]

Currently, the scattering performance of the foamed porous polymer structures is close to but still inferior to that of the

natural prototype, that is, of the *Cyphochilus* scales. This can be attributed to the pore structures well separated by thin walls, lacking interconnected and anisotropic characteristics.^[54] Further efforts should be devoted to foaming interconnected porous structures with a certain degree of anisotropy in the out-of-plane direction. In addition, the non-porous skin layers present in the foamed porous polymer films do not contribute to light scattering, which should be eliminated to improve the scattering ability.^[55]

3.2. Phase Separation

3.2.1. Non-Solvent-Induced Phase Separation

At present, non-solvent-induced phase separation (NIPS) is one of the popular methods for fabricating highly scattering porous polymers. In a typical process, the polymer is dissolved into a mixture containing a good solvent and a non-solvent, both of which are miscible.^[56] Note that the good solvent used for dissolving the polymer is usually volatile, while the non-solvent is less volatile. With the evaporation of the good solvent, the solubility of the polymer is reduced, and then phase separation between polymer and non-solvent occurs, leading to the formation of porous structures. As shown in **Figure 4a**, Syurik et al. directly casted PMMA-acetone solution in air for making highly scattering porous structures with an anisotropic fibril network.^[21] Due to the hygroscopic nature of acetone and intrinsic water in the PMMA, the transparent solution was turned into a solid white layer upon the complete evaporation of acetone. The phase separation between PMMA and water caused this effect. The scattering strength of the porous structures can be enhanced by tailoring the morphology of the porous structures, achieved by varying the PMMA's molecular weight. In the end, the artificial porous polymer film with a thickness of 4 μm featured a mean free optical path l_t as low as 1 μm at a wavelength of 500 nm, which outperformed the white beetle in the scattering performance for the first time. A similar recipe was adopted by Mandal et al. to fabricate porous poly(vinylidene fluoride-co-hexafluoropropylene) (P(VDF-HFP)) with bimodal pore size distributions, which were conducive to achieving broadband high scattering ability in the whole solar spectrum (300–2500 nm).^[37] The measured l_t of the porous P(VDF-HFP) with thicknesses above 300 μm was 6–12 μm in the wavelength range of 420–1100 nm. Later on, Zou et al. developed a 3.5 μm -thick porous PS film with an l_t below 1 μm at a wavelength of 500 nm, based on water vapor-induced phase separation.^[20] The outstanding scattering ability was attributed to the bi-continuous network of porous structures and the high refractive index of PS ($n \approx 1.6$). During the process, phase separation was induced by penetration of water vapor into the PS solution. Hence the underlying mechanism is slightly different from the above-mentioned evaporation-induced method. Recently, Burg et al. prepared a porous cellulose acetate (CA) film with a thickness of 12.8 μm , based on the non-solvent phase separation of a mixture containing CA/acetone/methanol/ CaCl_2 composite.^[11] The film exhibited a reflectance of $\approx 94\%$, surpassing that of *Cyphochilus* scales with a similar thickness. The research has unveiled the formation mechanism for the voided intra-scale structure as liquid-liquid

phase separation and further claimed a new optimal chitin filling fraction of 25%. The similar formation mechanism of porous structures made by the NIPS method to that of *Cyphochilus* scales might explain the fact that such artificial porous films possess comparable or even better scattering performance than their natural counterparts.

3.2.2. Polymerization-Induced Phase Separation

Light-scattering porous polymers can also be obtained from direct synthesis methodology, herein polymerization-induced phase separation (PIPS). The method is based on free-radical polymerization of mixtures containing monomers, porogens, and initiators, which is triggered by applied heat or UV irradiation.^[59,60] The porogens are miscible with the monomer precursor and can be extracted by solvent annealing after the polymerization process, thereby leaving behind abundant pores as scattering centers inside the polymer matrix. As shown in **Figure 4b**, Tang et al. first utilized the PIPS method for making highly scattering porous polymers based on the UV-induced initiation process, which has several advantages as it exhibits fast response and short polymerization time.^[57] The formulation contained monomers (i.e., butyl methacrylate (BMA) and ethylene dimethacrylate (EDMA)), porogenic solvents (i.e., cyclohexanol and 1-decanol), and a free-radical UV initiator. By leveraging the EDMA as the crosslinker of BMA, the copolymerization of BMA and EDMA produced a cross-linked poly(BMA-co-EDMA) matrix under the UV irradiation and led to the phase separation of polymer matrix and porogens. Two key parameters, including the volume ratios of 1-decanol to cyclohexanol and of porogens to monomers, were investigated in detail to tailor the morphology of as-prepared porous polymers. Finally, with an optimized pore diameter of ≈ 200 nm and a porosity of $\approx 50\%$, the porous polymer films with thicknesses ranging from 16 to 83 μm exhibited l_t values of 3–4.4 μm at wavelengths of 400–800 nm. Further, the same group made porous fluoropolymer films with thicknesses ranging from 14 to 55 μm , featuring l_t values of 1.3–1.7 μm in a wavelength range of 400–800 nm.^[33] The adopted fluorine monomer, namely perfluoropolyether (PFPE)-urethane dimethacrylate, combines the inherent properties of the PFPE backbone and methacrylate units to enable a low degree of shrinkage upon curing and a high level of cross-linking. This might be favorable for forming the compact porous structures with significant optical scattering effects. In addition, the as-made porous fluoropolymer films can be freestanding and flexible, which was not realized for the porous poly(BMA-co-EDMA) films. Note that the porous films obtained from the PIPS method contain open and interconnected porous networks, which are desired for post-encapsulation using another polymer. Liang et al. infiltrated a liquid PDMS precursor into porous poly(MMA-co-EDMA) films, achieving the fabrication of diffusing films with combined high transmittance and high haze (88%/88%) after a thermal curing process.^[61]

3.2.3. Polymer-Blend Phase Separation

Porous structures for optical applications can be generated from the phase separation of polymer blends since most polymer

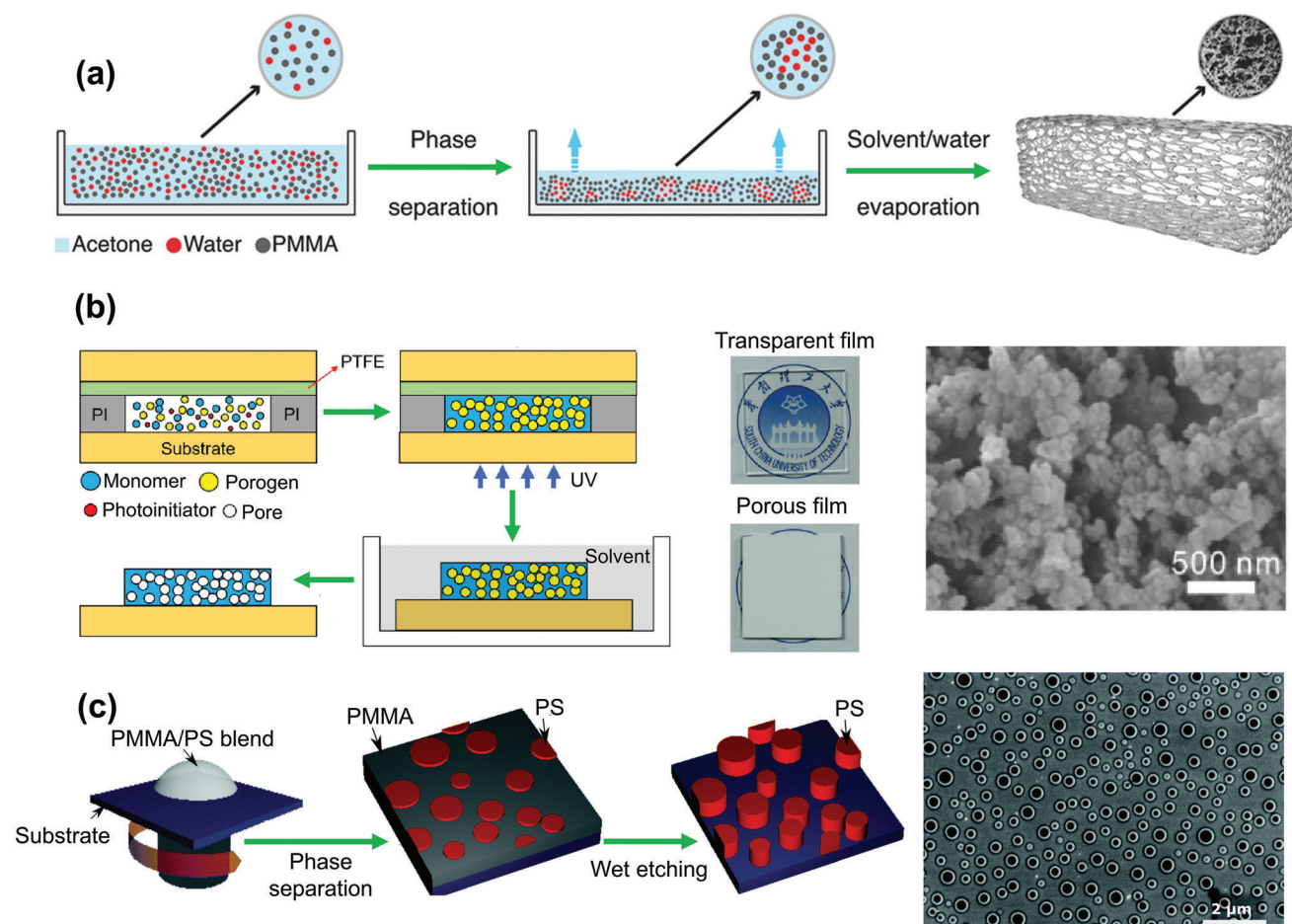


Figure 4. a) Schematic diagram of non-solvent-induced phase separation process and fibril morphology of porous PMMA film. The whole fabrication process is shown as follows: i) First, a three-phase mixture consisting of acetone, water and PMMA is prepared; ii) Then, the solution is subject to atmosphere for the fast evaporation of acetone, leading to the phase separation of water and PMMA; iii) Finally, a porous polymer film is obtained after the complete evaporation of acetone and water. Reproduced with permission.^[21] Copyright 2018, The Authors, published by Wiley-VCH. b) Schematic view of polymerization-induced phase separation process, photos of a transparent film and a white porous film and cross-sectional morphology of the porous film shown in the middle panel. The fabrication process contains four main steps: i) Preparing homogenous mixtures containing monomers, porogens, and a photoinitiator; ii) The cross-linking of monomers is initiated by UV irradiation, leading to the phase separation of the porogens and the cured polymer; iii) Extracting porogens by submerging the as-prepared polymer film in a good solvent bath; iv) Obtaining the porous film by air drying. In the right panel, we observe that the nonporous polymer film is transparent, whereas the porous film appears white due to light scattering effect. The right panel shows that the as-made porous structure consists of aggregated small globes separated by irregular air pores. Reproduced with permission.^[57] Copyright 2020, Optical Society. c) Schematic illustration of polymer-blend phase separation process and the morphology of disordered PS nanopillars. The left panel shows the whole fabrication process: i) A PMMA/PS blend solution is spin coated on a substrate; ii) The fast evaporation of the solvent leads to the separation between PMMA and PS; iii) By selectively dissolving PMMA, one obtains well-separated PS nanopillars. The right panel shows that the PS nanopillars have a disordered distribution without any overlap. Reproduced with permission.^[58] Copyright 2018, Royal Society of Chemistry.

blends of high-molecular-weight polymers are inherently immiscible.^[62,63] This effect can be utilized for fabricating polymer micro- and nanostructures. For example, phase separation occurs when the polymer blends are heated above the glass transition temperature or the solvent evaporates from the solution. This can result in tailored morphologies, including islands, holes, and bi-continuous structures. Note that the porous structures are usually 2D and can, for example, be tailored by varying the mixture composition, molecular weights of polymers, film thicknesses, or solvents. Alternatively, altering environment parameters, including air humidity and temperature, can be

used to control the process. Instead of using polymer blends, block copolymers can also be used for making phase-separated porous structures with refined self-assembled morphologies. However, the synthesis of block copolymers is fairly intricate, limiting their practical applications (e.g., anti-reflective layers). Intriguingly, the phase separation of polymer blends (or block copolymers) can generate either disordered or ordered porous structures. The ordered porous structures tend to produce some structural color effects, which is beyond the scope of this article and can be referred to in a recent review article.^[42] For broadband optical scattering applications, disordered structures are more

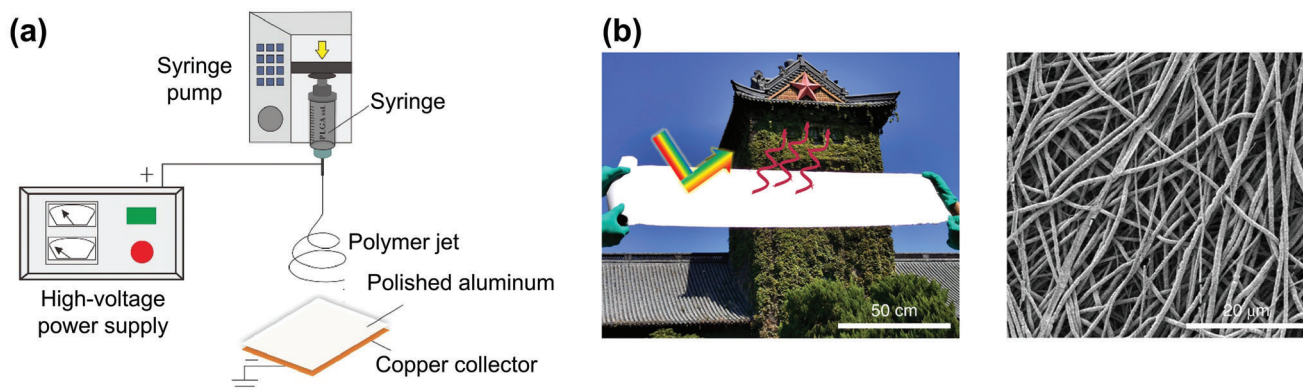


Figure 5. a) Schematic diagram of electrospinning setup containing a high-voltage power supply, a syringe, and a grounded metallic collector. Reproduced with permission.^[69] Copyright 2017, Optical Society. b) Highly reflective electrospun PEO film with a thickness of 500 μm (left) and its fibrous morphology observed by SEM (right). Reproduced with permission.^[72] Copyright 2020, The Authors, published by Springer Nature.

relevant. As shown in Figure 4c, in the work by Donie et al., a polymer blend of PMMA and PS was spin-coated on substrates, followed by phase separation of these two polymers initiated by solvent evaporation.^[58] After selectively dissolving the PMMA by using acetic acid, the porous structures, namely air with some PS nanopillars inclusions, were fabricated. To foster significant scattering effects in the visible and near infrared spectral range, the polymer blend composition and the deposition conditions were adjusted to tune the morphology of the phase-separated nanostructures (i.e., the shape, the diameter, and the height distribution of nanopillars). At last, the best scattering performance was realized by nanopillars with a mean diameter of 357 nm, an average height of 80 nm, and a surface cover range of 30%. With the conformal deposition of silver onto the porous film, a diffuse reflector for a thin-film silicon solar cell was made. The authors characterized its light-scattering performance using haze, defined as the proportion of diffused light in total reflected light. It was shown that a maximum haze value surpassing 85% was realized under various incidence conditions.

The phase-separated porous polymers can be further processed to generate disordered titania nanopillars for light extraction of OLEDs.^[64] In addition, by using an inorganic-organic hybrid UV-curable resin, (i.e., OrmoStamp), the obtained porous polymer scaffold can serve as a nano-stamp for imprinting nanostructures, confirming the versatility and up-scalability of the polymer-blend phase separation method.^[65]

3.3. Electrospinning

Electrospinning is a well-established nanofiber production technique that applies high electric field to draw charged threads with a size in the order of hundreds of nanometers to micrometers from polymer solutions. In a typical electrospinning process, as shown in Figure 5a, a sufficiently high voltage is applied to a liquid droplet for charging it. Then the droplet is stretched under the influence of the electric field, forming a jet in air. The jet is elongated and thinned by a whipping process combined with solvent evaporation until it is ultimately deposited on the grounded metallic collector. The uniform distribution and high anisotropy in the out-of-plane direction of electrospun films are

desired for realizing highly scattering performance. Yip et al. first produced electrospun PU nanofiber webs with a brilliant CIE whiteness index exceeding 85 (note that the CIE index of whiteness is a measurement of the light reflected by the sample across the visible spectrum). This was achieved by optimizing processing parameters including solvent, polymer concentration, and collection geometry to obtain an interconnected fiber network with a mean fiber diameter of around 250 nm.^[66] To date, many polymers have been electrospun for making high-scattering porous films, including polyacrylonitrile (PAN),^[67,68] poly(lactic-co-glycolic acid),^[69] PS,^[27,28] and PVDF.^[70,71]

As shown in Figure 5b, Li et al. prepared a highly reflective nanofibril polyethylene oxide (PEO) film with a thickness of 500 μm and an average fiber diameter of 730 nm by electrospinning, resulting in a high reflectance of 96% over the solar spectrum (300–2500 nm).^[72] The authors demonstrated that the selected fiber diameter was an optimized value based on their scattering efficiency calculation for a single fiber. In contrast, Yalçın et al. verified the optimal size of electrospun fibers as 400–500 nm at a film thickness smaller than 1 mm by solving the radiative transfer equation (RTE) with the Monte Carlo method.^[73] The discrepancy between the two studies demonstrated the importance of a rigorous method for solving the RTE for optimizing the diameter.^[51] In addition, Park et al. determined that the maximum reflection of their electrospun nano silk film was achieved with a mean fiber diameter of 250 nm over a wavelength range of 400–900 nm by using a rigorous anisotropic photon diffusion theory.^[51] The results showed that the optimal fiber size for maximizing scattering performance depended on the light wavelength of interest. Their simulation also pointed out that further optimization of the filling fraction can lead to enhanced scattering performance for the electrospun film. Besides the size and the filling fraction of electrospun fibers, the fiber morphology also has a critical effect on the scattering properties. Kim et al. demonstrated that electrospun fibers with hybrid cylindrical and ellipsoidal shapes exhibited stronger scattering abilities than those with only cylindrical shape.^[74] The underlying mechanism was that the scattering cross section of a hybrid fiber was summed from the individual cross sections of cylindrical fiber and ellipsoidal fiber, indicating that composite fibers could scatter broadband light more efficiently than their counterparts with

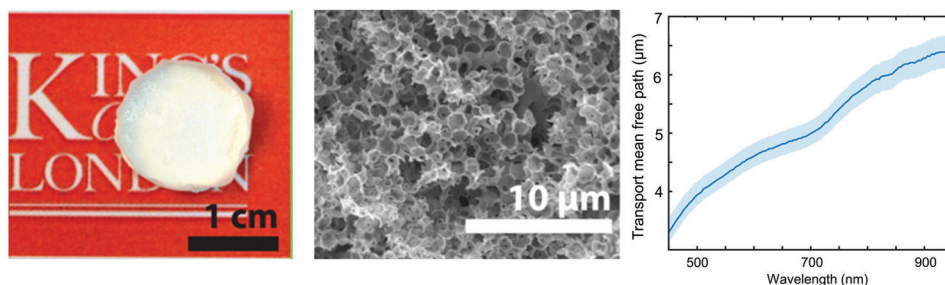


Figure 6. Porous cellulose nanocrystals film and its scattering performance. Left: Photo of the white porous cellulose film (100 μm thick), middle: SEM image of its inner porous morphology, right: spectral dependence of the transport mean free path l_t in the visible spectral range 450–950 nm. Reproduced with permission.^[80] Copyright 2017, The Authors, published by American Chemical Society.

a single shape. Their results provide new insights to enhance the scattering ability of porous films made by electrospinning. Recently, electrospun films, featuring a transport mean free path of 0.9 μm , have surpassed *Cyphochilus* scales in the optical scattering strength for the first time, which were optimized to mimic the key structural parameters of the beetle scales (i.e., mean fiber diameter, diameter distribution, filling fraction, and structural anisotropy).^[75]

In addition, electrospun porous films featuring open and interconnected networks are also suited for secondary encapsulation to enable the fabrication of optical diffusers. Lee et al. produced a composite diffuser with transmittance/haze of 67%/66% by infiltrating transparent photoresist SU-8 into an electrospun nanoporous PAN film.^[76] The diffusing properties can be well tailored by tuning the concentration of polymer solution and film thickness. Similarly, Tang et al. produced electrospun PVDF-based diffusers encapsulated by UV-curing resin, featuring combined transmittance/haze of 78% and 92%, respectively.^[77] In a recent study, Liang et al. showed that the electrospun PS film could be tailored into PS-fiber rods with different lengths by using an emulsion shear process. Their work resulted in varied scattering abilities dependent on the obtained fiber length.^[78] With further encapsulation by PDMS, the composite diffusing film realized a high haze of 87% while maintaining a high transmittance of 82% at a wavelength of 550 nm.

3.4. Direct Templating

Porous polymers can be produced by direct templating, which is inherently a molding technique for the direct replication of the complementary structure of porous templates with well-defined morphology, followed by the removal of the templates for forming the ultimate porous structure.^[79] The commonly-used templates for making porous polymers include polymer nanoparticles, silica nanoparticles, and anodic aluminum oxide. As shown in **Figure 6**, Caixeiro et al. prepared a high-scattering cellulose nanocrystals film by using colloidal monodisperse PS spheres (diameter of 1.27 μm) as a sacrificing template.^[80] The as-fabricated porous films with thicknesses ranging from 100 to 400 μm featured a l_t as low as 3.5 μm in the visible light range, showing a significantly improved scattering strength ($\times 4$) compared to conventional microfiber-based paper. A detailed Mie scattering modeling further demonstrated that a decrease-

ing sphere diameter to 250 nm can result in enhanced scattering performance corresponding to an optical mean free path l_t of 1.3 μm . A similar strategy could also be applied to fabricate porous PDMS films. For instance, Zhou et al. prepared a white porous PDMS sponge using sugar particles with a size of 100–600 μm as templating materials.^[81] The as-fabricated porous film had needed to have a thickness of 5 mm to exhibit a reflectance exceeding 90% in the visible range, indicating its insignificant scattering ability. It is intuitive to use particles with a smaller size to realize stronger scattering performance. Weng et al. synthesized NaCl particles with an average size of around 5 μm using the solvent method, which were used as templates for fabricating porous PDMS films.^[82] Ultimately, a 450 μm -thick porous film featuring an average reflectance of $\approx 95\%$ in the solar spectrum was obtained. It is evident that the reduced template size leads to a stronger scattering ability for the porous PDMS film. However, removing finer sugar particles from the polymer matrix can take a much longer time. To enable a highly efficient process for making porous PDMS films, Zhou et al. adopted a self-assembled PS array with a particle size of 1 μm as the sacrificial template of PDMS.^[83] The removal of PS microspheres was achieved by a simple annealing process in an oven (180 $^\circ\text{C}$ @3 h). In addition, they verified that porous films with 1 μm -sized pores featured stronger scattering abilities than those with 5 μm -sized pores. The results might explain the fact that the above-mentioned porous cellulose films have a similar pore size.

Note that one drawback of conventional direct templating is that the template materials need to be removed by further dissolution in a good solvent bath, which is usually time-consuming and cumbersome. To circumvent the dissolution step, researchers harnessed breath figure self-assembly as a cost-effective, time-saving, and facile templating method for making porous polymers.^[84] In a general breath figure process, a polymer solution is first cast onto a solid substrate by spin or dip coating, which is subject to a humid atmosphere. With the solvent evaporation from the uncured polymer film, its surface temperature decreases gradually due to the evaporation cooling effect. Further, water vapor can condense onto the polymer surface spontaneously, forming numerous water droplets as the templating materials for the polymer when the temperature is well below the dew point of water. After the solvent and the water droplets evaporate completely, a porous polymer film is obtained. The formed porous array usually has a honeycomb-shaped distribution, which can efficiently scatter incident light and serve as light

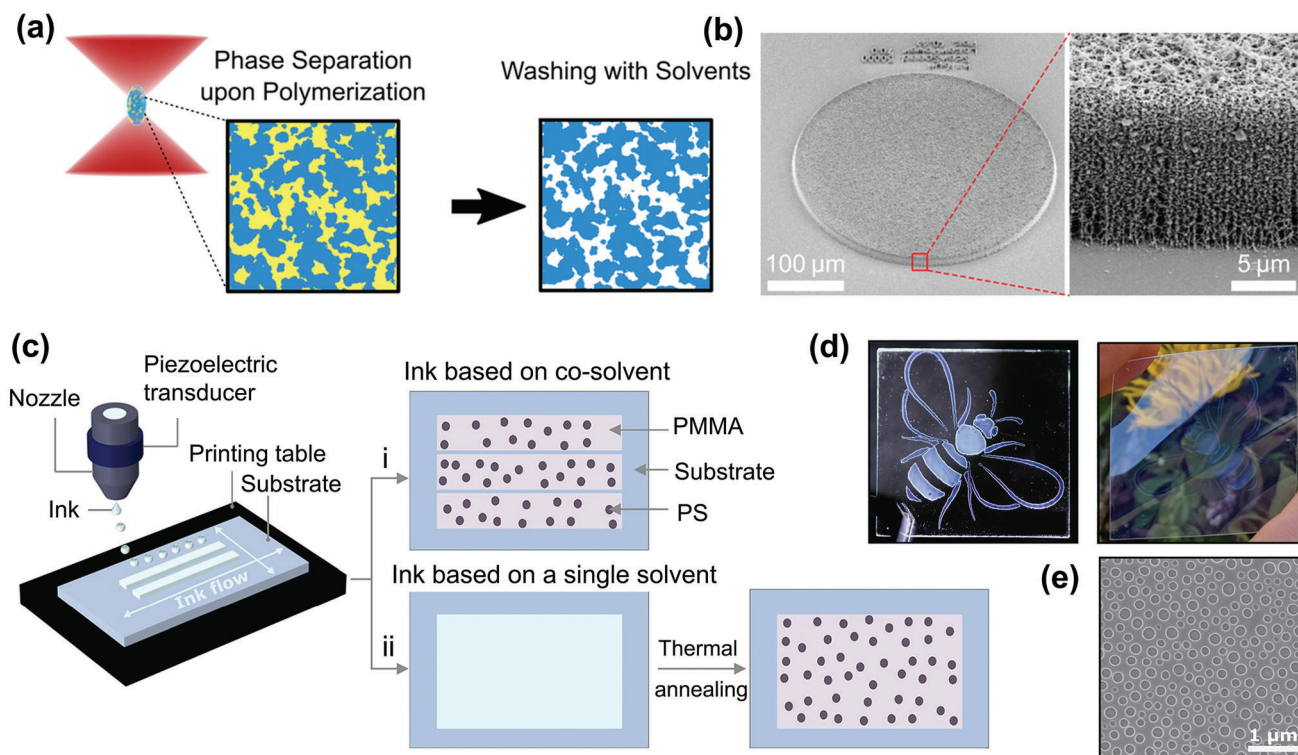


Figure 7. a) Schematic diagram of two-photon laser microprinting combined with polymerization-induced phase separation for making porous polymers. In a polymerization process enabled by two-photon laser microprinting, phase separation between polymer and porogens occurs, leading to porous morphology in the polymer matrix. After washing with solvents and a drying process, a porous polymer film is obtained. The as-prepared polymer film features an interconnected nanoporous morphology. b) SEM images of a nanoporous sample made by two-photon laser microprinting. Reproduced with permission.^[87] Copyright 2020, The Authors, published by Wiley-VCH. c) Schematic view of inkjet printing combined with polymer-blend (PMMA/PS blend) phase separation for making 2D porous structures. The inkjet printing process is either based on i) a co-solvent recipe (cyclohexanone and Tetralin) or ii) a single-solvent formulation (only cyclohexanone). The co-solvent recipe enables the phase separation of the polymer blend without further treatment, whereas thermal annealing is required to initiate the phase separation process. d) Photographs of inkjet-printed bee logos on a glass substrate (left) and on a flexible plastic substrate (right). e) SEM image of disordered nanoholes with a uniform distribution. Reproduced with permission.^[88] Copyright 2021, American Chemical Society.

outcoupling layers for optoelectronic devices.^[85] In addition, the concave-shaped porous array formed by the breath figure technique can be leveraged as a template for making convex-shaped structures.^[86]

3.5. Printing Methodology

To enable facile and tailorable fabrication of porous polymers, combining the pore-forming process with advanced printing methodology is of great interest. It is also particularly intriguing to introduce the scattering properties over well-defined 2D or 3D designs by using printing techniques. As shown in **Figure 7a**, Mayer et al. demonstrated a two-photon absorption-based 3D laser microprinting approach combined with the PIPS for making porous polymers, which enabled better spatial resolution of patterning and achieved nanoporous architectures with controlled pore sizes ranging from the scale of ten nanometers to the micrometer scale.^[87] In this approach, organic solvents including dodecyl acetate and octadecyl acetate, which are miscible with the unpolymerized monomers, were applied as porogens for the PIPS. Since the miscible porogens enabled a homoge-

neous refractive index distribution throughout the volume, the light scattering effect that hinders the accuracy of the two-photon absorption-based 3D printing would be avoided during the process. As presented in **Figure 7b**, a nanoporous polymer structure with a mean pore size around 50 nm was fabricated. Controllable porosity of the structure was achieved by manipulating the power level during exposure. It was shown that increasing laser power from 30 to 45 mW resulted in a porosity decrease from 43% to 22%. This further enabled the fine control of the light scattering effect of the printed sample. Consequently, a miniaturized Ulbricht light-integrating sphere with excellent diffuse reflectivity was fabricated by this approach for demonstrating the excellent scattering performance.

Inkjet printing is an efficient printing technique for the direct deposition of liquid phase materials on a variety of substrates, attracting a wide variety of scientific and industrial attention owing to its high adaptability, cost efficiency, and scalability for mass production. Novel ink design and process development have been adapted to inkjet printing technology for creating tailored porous structures. As shown in **Figure 7b**, the polymer blend solution of PMMA and PS was directly inkjet printed by Donie et al. to induce phase separation upon solvent

Table 1. Comparison of scattering performance of various porous polymers in previous publications.

Type of porous polymers	Refractive index at 500 nm	Fabrication method	I_t at specific wavelength	Reference
White beetle <i>Cyphochilus</i> scales	1.56	—	1.47 μm at 500 nm	[9]
Porous PMMA film	1.5	Microcellular foaming	3.5–4 μm (400–800 nm)	[7]
Porous PMMA film	1.5	Non-solvent-induced phase separation	1 μm at 500 nm	[21]
Porous P(VDF-HFP) film	1.4	Non-solvent-induced phase separation	6–12 μm at 420–1100 nm	[37]
Porous PS film	1.6	Non-solvent-induced phase separation	0.98 μm at 500 nm	[20]
Porous cellulose acetate film	1.5	Non-solvent-induced phase separation	<1.47 μm at 500 nm	[11]
Porous Poly(BMA-co-EDMA) film	Not reported	Polymerization-induced phase separation	3–4.4 μm at 400–800 nm	[57]
Porous fluoropolymer film	Not reported	Polymerization-induced phase separation	1.3–1.7 μm at 400–800 nm	[33]
Porous nano silk film	1.55	Electrospinning	\approx 5 μm at 400–900 nm	[51]
Porous nano silk film	1.55	Electrospinning	0.9–2.1 μm at 400–700 nm	[75]
Porous cellulose nanocrystals film	1.5	Direct templating	3–7 μm at 450–950 nm	[80]

evaporation, thereby forming a 2D porous structure followed by a selective dissolving procedure.^[88] The printed bee logos shown in Figure 7c demonstrated that the formed nanoporous structures (see Figure 7d) were fairly homogeneous. Processing parameters including printing resolution, the weight ratio of PS/PMMA, and thermal annealing temperature, were investigated in detail to enable the morphological variation of the porous structures scaling from a few micrometers down to sub-100 nm range. With the inkjet printing methodology, the 2D porous structures can be rapidly processed into the target macroscopic design with tailored scattering performance.

It is well noted that porous polymers can also be fabricated by other common printing methods, including direct ink writing^[89] and digital light processing.^[90–92] To enable the fabrication of porous polymers with efficient light-scattering strength, those printing methodologies need to be optimized for obtaining desired porous structures.

To get more insights into the current development of light-scattering porous polymers, a list shown in Table 1 was prepared for comparison of their scattering performances. The list contains the type of porous polymers (including the benchmark of white beetle *Cyphochilus* scales), refractive index, fabrication method, and corresponding I_t . We note that some artificial porous polymers have surpassed the white beetle scale in terms of scattering strength, as evidenced by the I_t . This achievement indicates a bright and promising future for making light-scattering porous polymers with more advanced methodologies.

4. Applications

4.1. Optoelectronic Devices

4.1.1. Optical Enhancement of LEDs and OLEDs

LEDs (herein referred to as inorganic LEDs, i.e., GaN-based LEDs) and OLEDs suffer from limited efficiencies due to the large refractive index of their constituent materials compared to that of air.^[93–95] A significant fraction of the internally generated light is trapped inside the devices due to the coupling to guided modes. By integrating scattering layers into LEDs or OLEDs, the

trapped modes can be effectively extracted from the devices, contributing to a large enhancement of the efficiencies.^[76] As shown in Figure 8a, Yu et al. demonstrated the light-extraction ability of porous films made by the PIPS method by integrating white scattering layers onto the substrates of chip-on-board LEDs with a near-Lambertian light distribution.^[33] In the LED device with porous films, the total internal reflection light can be reflected in a diffusing way instead of the specular direction, which increased the photon escape probability and thereby improved the light extraction efficiency of the device by 20%. Similar enhancement can be implemented by inserting an electrospun PS film; this was demonstrated by Liang et al.^[96] Highly diffuse reflective layers can also be integrated onto the reflectors of LED lamps to enhance their light extraction efficiency, alleviate the glare effect and improve the angular color uniformity. Tang et al. integrated an electrospun PLGA film onto the reflector surface of a remote-phosphor-converted LED lamp, which reduced the correlated color temperature deviation significantly while achieving an efficiency gain of 12%.^[69] Note that the uniform mixing of blue and yellow light from the LED lamp was realized by the excellent light-scattering effect of the electrospun film. Furthermore, the same group demonstrated the versatility of light-scattering porous polymer films by integrating electrospun PAN films onto various LED lamps, leading to similar light efficiency enhancements.^[68]

The non-cavity planar OLEDs suffers from a limited outcoupling efficiency of only 20–30% due to surface plasmon loss mode at the planar organic-metal interface and laterally propagating waveguided and substrate-trapped loss modes stemming from the refractive index contrasts in the device, starting from high-index organic matrices to a medium-index glass substrate to low-index air.^[34,64] The insertion of a scattering layer onto the glass substrate represents a promising route to effectively extract substrate modes. By leveraging the phase inversion method, Koh et al. developed a thin light-scattering porous polyimide film with a high-index matrix ($n > 1.7$) to improve the outcoupling efficiency of green and broadband OLEDs by 65% and 60%, respectively, as shown in Figure 8b.^[34] The improvements were enabled by a significant scattering effect induced by the large index contrast between polyimide matrix and air pores as well as the fact that the index of polyimide was larger than that of the

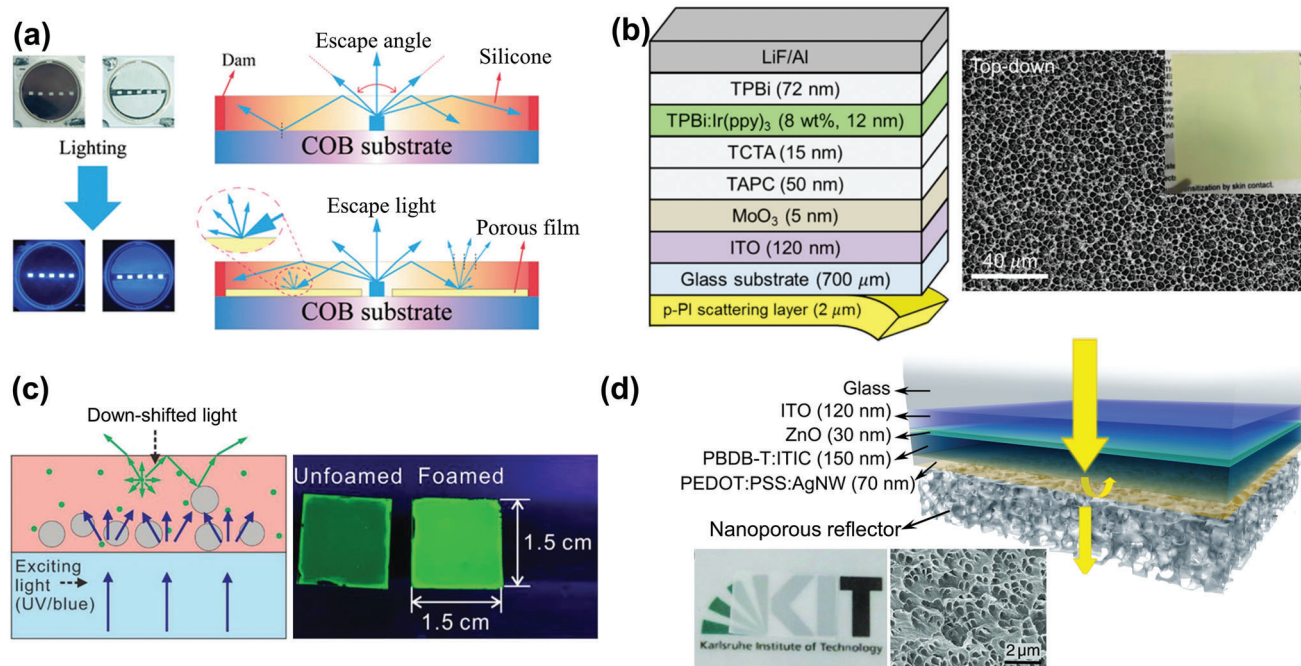


Figure 8. a) Reference LED without a porous film and LED with a porous film serving as a diffuse light reflector as well as the illustration of the light extraction mechanism. Reproduced with permission.^[33] Copyright 2021, Wiley-VCH. b) Device structure of the green OLED with a porous polyimide film as the light-outcoupling layer and the top-down confocal microscopy image (the inset is a photograph of the porous polyimide film). Reproduced with permission.^[34] Copyright 2015, American Chemical Society. c) Schematic illustration of PL intensity enhancement of QD film owing to the assistance of the micropores and photograph of unfoamed and foamed QD films under UV light excitation. Reproduced with permission.^[35] Copyright 2019, Wiley-VCH. d) Schematic diagram of OSC integrated with a nanoporous polymer film on the rear side as a diffuse light reflector. Reproduced with permission.^[36] Copyright 2021, The Authors, published by Wiley-VCH.

glass substrate, which was conducive to outcoupling substrate-trapped light into the porous polymer layer. Furthermore, the adopted porous layer can also enhance the color consistency between viewing angles of 0° and 60°. Yun's group demonstrated that the choice of alcohols instead of water in the phase inversion method played an important role in implementing uniform pore size with well-controlled pore shape. This allowed to control the light scattering effect and ray path change of porous polymer films, thereby largely enhancing the outcoupling efficiency of OLEDs.^[97] By further tuning the mixing ratios of different non-solvents (i.e., water and ethanol), the light scattering effect of the porous polyimide films can be precisely tuned, thereby realizing a larger efficiency enhancement for OLEDs.^[98]

4.1.2. Photoluminescence Intensity Enhancement of Color Conversion Layers

The photoluminescence (PL) intensity of fluorescence materials can benefit from the lengthened photon transport path of excitation light inside the porous polymer films as well as light extraction from the top-emitting surface of the films.^[99–101] Aiming at improving the PL intensity of PMMA/quantum dot (QD) hybrid films, Yu et al. introduced tailored porous networks inside these hybrid films via supercritical CO₂ microcellular foaming method to increase the scattering effect, as shown in Figure 8c.^[35] By employing spectroscopic measurements, it was found that the

PL intensity of the porous QD film was enhanced nearly seven-fold compared to the pristine QD film with a thickness of 4 μm. The measured spectroscopic results demonstrated that both the absorption and PL quantum yield enhancement contributed to the ultimate improvement of PL intensity. Note that by substituting the pristine PMMA with one with a high molecular weight, nanoporous PMMA films can be fabricated, which exhibited a stronger scattering ability than the microporous ones. However, the PL enhancement factor upon the introduction of nanoporous network was inferior to that with the microporous morphology, which might be attributed to the strong backscattering ability.^[54] Similarly, Jung et al. prepared QD composite films by encapsulating QD into porous block copolymer matrix by using water-vapor-induced phase separation method, which enabled a 21-fold PL intensity enhancement over a broad spectral range.^[102] In this work, the polymer-QD composite with bi-continuous random pores realized effective enhancement of both light absorption and extraction efficiency via efficient light scattering effect. Moreover, the phase-separated morphology substantially reduced the Förster resonance energy transfer efficiency from 53% (pure QD film) to 22% (polymer-QD composite), which further enhanced the PL intensity of QD film. Apart from directly generating pores inside the QD films, infiltrating liquid QD-polymer composites into porous scaffolds is also a feasible route to form scattering centers. For example, Liang et al. demonstrated a 1.5-fold enhancement in the PL intensity of QD films with the use of porous polymer scaffolds made by the PIPS method.^[61] Moreover, the

enhancement factor was increased twofold by using electrospun PS nanofibers.^[78]

4.1.3. Nanoporous Polymer Reflector for Solar Cells

Metal electrodes are usually integrated as the back electrodes of conventional solar cells for charge transport and optical path length enhancement. This is a challenge for fully solutions processed low-cost solar cells realized by printing technologies. It represents a feasible and promising route to use highly conductive polymers to replace commonly adopted evaporated metals as the back electrodes of organic solar cells (OSCs), given the printability of such conductive materials. Although this route is well established to implement semitransparent solar cells that can be adopted for window applications, the insignificant reflectance of the polymer electrodes reduces light recycling and hence the power conversion efficiency (PCE) of OSCs. To enhance the light recycling part in the OSCs, porous polymer layers are good candidates to serve as the back reflectors of OSCs. In the work by Yu et al., a nanoporous polymer layer made by supercritical CO₂ microcellular foaming was integrated onto the rear side of OSC together with a conductive polymer electrode, as displayed in Figure 8d. By varying the thickness of pristine polymer film, different reflectance can be obtained, which is desired for the light management of semi-transparent OSCs.^[36] At last, a 50 μm-thick foamed polymer film can increase the PCE of OSCs from 5.9% to 6.8%, comparable with the highly reflective silver electrode. Detailed characterizations showed that the PCE enhancement was attributed to the increased light absorption in the low-absorbing spectral range and further improved photocurrent in the OSCs.

4.2. Passive Radiative Cooling

To alleviate energy consumption for cooling and reduce carbon footprint, a promising technique, namely passive daytime radiative cooling (PDRC), has been arising to cool down buildings in the daytime with hot weathers since the first introduction in 2014 by Fan's group.^[103] The radiative cooler leverages the 3 K universe as the radiative heat receiver. The cooling process is spontaneous and occurs without any energy input, which is green and low-cost compared with conventional air-conditioning technologies. However, realizing daytime radiative cooling is quite challenging since it requires both high reflectance in the solar spectrum (0.3–2.5 μm) and high emissivity in the atmosphere window (8–13 μm) to reduce solar light absorption and radiate mid-infrared emission, respectively. In recent years, light-scattering porous polymers have attracted much attention as potential daytime radiative coolers due to their intrinsically low solar absorbance, high mid-infrared emissivity, facile large area preparation, low costs, and easy integration. As shown in Figure 9a, Mandal et al. prepared hierarchically porous P(VDF-HFP) polymer coatings (solar reflectance: 0.96; long-wave infrared emittance: 0.97) by using a simple and scalable phase inversion method, which enabled a sub-ambient temperature drop of ≈6 °C and a cooling power of 96 W m⁻².^[37] Hu's group developed a super-strong cellulose material with excellent solar reflectance and mid-infrared emittance as well as mechanical strength of 404 MPa that showed great application potential as a structural engineering material

with outstanding PDRC capacity.^[104] It is noted that an increasing number of porous polymers have been developed for PDRC applications, including porous PMMA film,^[105] porous polytetrafluoroethylene film,^[106] porous PDMS film,^[107] porous PE film,^[108,109] porous PEO film.^[72]

Passive cooling with porous polymers is also a promising strategy for effective personal thermal management of individuals. As shown in Figure 9b, Cui's group showed that nanoporous polyethylene (nanoPE) was transparent to mid-infrared human body radiation while opaque to visible light due to the randomly distributed nanopores with the pore size ranging from 50 to 1000 nm.^[38] They demonstrated that the processed nanoPE can cool down the simulated skin temperature in a more effective way than conventional textile materials (e.g., cotton). Furthermore, the same group realized large-scale extrusion of continuous nanoPE microfibers that can be processed into fabrics with opaque visible appearance and high transparency in the mid-infrared spectra.^[110] Compared to a conventional cotton fabric with the same thickness, the nanoPE fabric showed a larger cooling power and a human skin temperature drop of 2.3 °C, corresponding to a 20% energy saving on the indoor cooling. In addition, the nanoPE film can also be used for the thermal management of nanofiber-based face masks.^[111] Note that the cooling concept of nanoporous PE is different from the classic PDRC mentioned above since the PE is not the thermal emitter, which limits the application range due to the specific choice of such material. To extend the application range of textiles in personal thermal management, a hierarchical-morphology fabric was proposed to serve as an effective and scalable radiative cooler with combined high solar reflectance and high mid-infrared emittance.^[112]

5. Summary and Outlook

This review first discussed suitable natural and artificial polymer materials for making light-scattering porous structures and their optical characteristics. Furthermore, several fabrication techniques that can produce high-scattering porous polymers were highlighted, including microcellular foaming, phase separation, electrospinning, and direct templating. With the combination of printing technologies and the pore-forming process, porous polymers can be made in a scalable and tailored way. We have also discussed several typical applications, which are mainly grouped into two scenarios (i.e., optoelectronic devices and passive radiative cooling). It is noted that with advanced fabrication methods and careful structure tailoring, the presented porous polymers possess prominent scattering abilities, some of which exhibit even stronger scattering performance than the best natural counterpart, namely the white beetles of the genus *Cyphochilus*. Although porous polymers have been studied for a long time, their optical characteristics and related optical applications are just in the infant stage. As an outlook for this review, we provide some perspectives as follows: 1) At present, most porous polymers are limited to several available commercial or natural polymer materials, which can be explored more to enable even stronger scattering abilities. Given the diversity of pore generating methods, more fabrication techniques can be developed to produce advanced light-scattering porous polymers. In

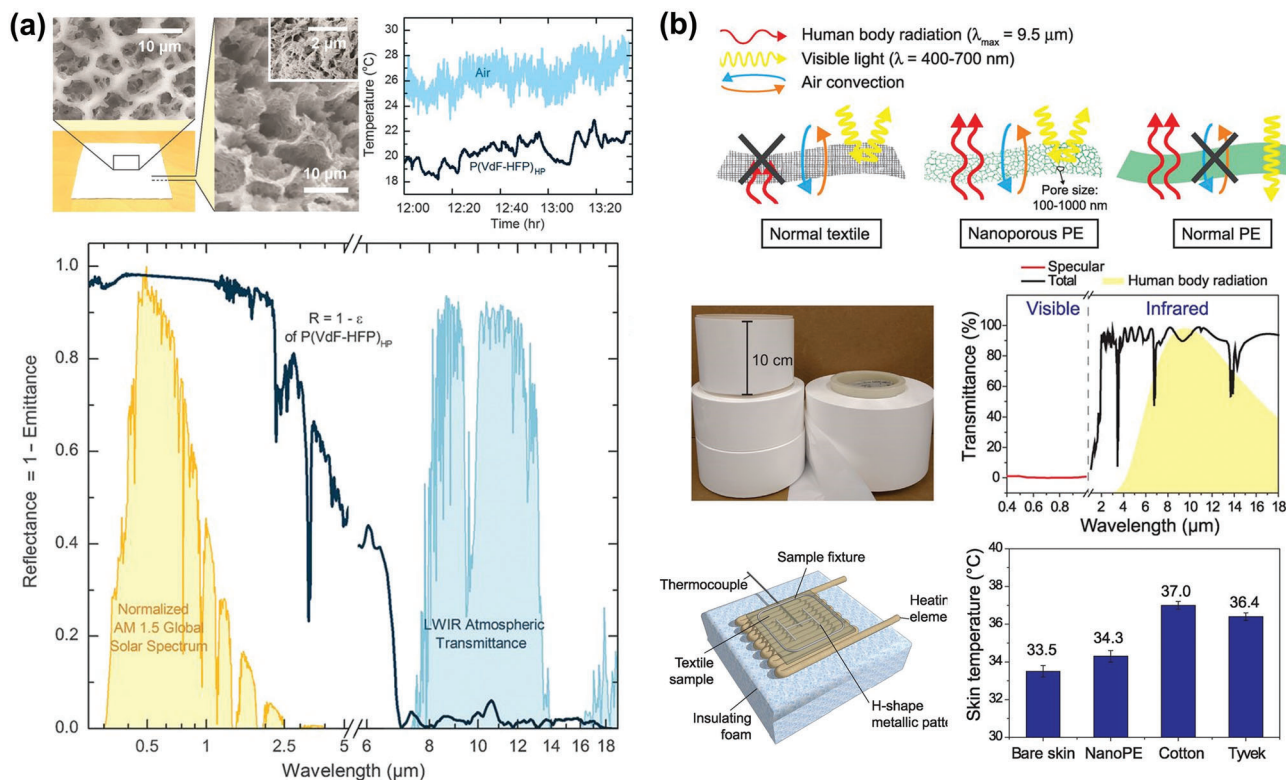


Figure 9. a) Hierarchical porous P(VdF-HFP) films with high solar reflectance and high mid-infrared emittance and their spectral properties as well as cooling performance. Reproduced with permission.^[37] Copyright 2018, American Association for the Advancement of Science. b) Nanoporous PE film with high visible reflectance and high mid-infrared transparency and their spectral properties and skin cooling performance. Reproduced with permission.^[38] Copyright 2016, American Association for the Advancement of Science.

addition, the mechanical strength of optical porous polymers is usually omitted in the current research, whereas it is mandatory for practical applications and should be carefully investigated. More functions or properties can be integrated into the light-scattering porous polymers for specific applications, such as water-repelling property (outdoor self-cleaning applications) and air permeability (textiles for human body cooling).^[113,114] Furthermore, the as-developed optical porous polymers can be applied to new scenarios, such as interfacial solar steam generation that utilizes porous materials as photothermal layers.^[115,116]

2) To understand the light scattering mechanism of the porous polymers and provide reasonable guidelines for the structure design, more advanced optical modeling and simulation is needed for the reported porous polymer structures, especially when considering the complexity of multiple scattering effects occurring in the porous media. There exist various scattering theories that can describe the scattering effects of porous polymers. The well-known Mie theory is suitable for simulating single spherical pore and infinite cylindrical pore with high accuracy and fast calculation.^[73] In terms of porous structures with complex irregular shapes, finite differential time-domain (FDTD) and finite element analysis (FEA) are usually adopted.^[117] However, the FDTD and FEA methods require significant computational resources and time, especially for those large-size porous structures.^[118] To alleviate the calculation burden, the T-matrix method is applied and shows good accuracy in simulating large

disordered nanoporous structures with reasonable simulation time.^[119] Note that the aforementioned methods can account for the wave-optical phenomenon, whereas it is impractical to simulate huge porous structures by using those methods. It would be helpful to resolve such issues by solving the well-established RTE. In this regime, Monte Carlo ray tracing can be used for the simulation of bulk porous media.^[73] Note that diffusion theory has also been developed to solve the RTE for reducing simulation time at an acceptable accuracy.^[51] We note that there exist no one-fits-all methods for simulating the light scattering effects of porous polymers. Therefore, we call for more efforts to be devoted to the simulation tasks, which should provide us with more insights into the interesting scattering effects of porous polymers. The interplay of materials research and predictive simulation would open new paths to more porous polymers with desired optical scattering properties.

Acknowledgements

S.Y. and J.C. contributed equally to this work. This work was supported by the One-Hundred Talents Program of Sun Yat-sen University, Guangzhou Science and Technology Research Project (202102020822), China Postdoctoral Science Foundation (2020M672618), the Open Fund of Hubei Key Laboratory of Mechanical Transmission and Manufacturing Engineering at Wuhan University of Science and Technology (MTMEOF2020B02), and the Open Project of Guangdong Provincial Key Laboratory of Technique and Equipment for Macromolecular Advanced Manufacturing (2021kfkt01) as

well as International Training Program (Postdoctoral Program) for Young Excellent Talents of Guangdong Province. J.C. acknowledges the Ph.D. fellowship offered by China Scholarship Council to support his study at KIT. G.G., H.H., and U.L. acknowledge financial support through the SPP 1839/2 “Tailored Disorder—A science- and engineering-based approach to materials design for advanced photonic applications” of the German Science Foundation (DFG). This research was also funded by the Deutsche Forschungsgemeinschaft (DFG, German Research Foundation) under Germany’s Excellence Strategy via the Excellence Cluster 3D Matter Made to Order (EXC-2082/1—390761711). This article is part of the Advanced Optical Materials Hall of Fame article series, which recognizes the excellent contributions of leading researchers to the field of optical materials science.

Open access funding enabled and organized by Projekt DEAL.

Conflict of Interest

The authors declare no conflict of interest.

Keywords

bioinspired optical materials, light scattering, optoelectronics, phase separation, porous polymers, radiative cooling

Received: December 29, 2022

Revised: February 21, 2023

Published online:

- [1] D. S. Wiersma, *Nat. Photonics* **2013**, 7, 188.
- [2] S. Yu, C.-W. Qiu, Y. Chong, S. Torquato, N. Park, *Nat. Rev. Mater.* **2021**, 6, 226.
- [3] S. Dou, H. Xu, J. Zhao, K. Zhang, N. Li, Y. Lin, L. Pan, Y. Li, *Adv. Mater.* **2020**, 33, 2000697.
- [4] L. Pattelli, A. Egel, U. Lemmer, D. S. Wiersma, *Optica* **2018**, 5, 1037.
- [5] Y. Tang, Z. Li, Z.-T. Li, J.-S. Li, S.-D. Yu, L.-S. Rao, *IEEE Trans. Electron Devices* **2018**, 65, 158.
- [6] L. Rao, Y. Tang, Z. Li, X. Ding, J. Li, S. Yu, C. Yan, H. Lu, *Opt. Express* **2017**, 25, A432.
- [7] J. Syurik, R. H. Siddique, A. Dollmann, G. Gomard, M. Schneider, M. Worgull, G. Wiegand, H. Hölscher, *Sci. Rep.* **2017**, 7, 46637.
- [8] P. Vukusic, B. Hallam, J. Noyes, *Science* **2007**, 315, 348.
- [9] M. Burrelli, L. Cortese, L. Pattelli, M. Kolle, P. Vukusic, D. S. Wiersma, U. Steiner, S. Vignolini, *Sci. Rep.* **2014**, 4, 6075.
- [10] G. Jacucci, J. Bertolotti, S. Vignolini, *Adv. Opt. Mater.* **2019**, 7, 1900980.
- [11] S. L. Burg, A. Washington, D. M. Coles, A. Bianco, D. McLoughlin, O. O. Mykhaylyk, J. Villanova, A. J. C. Dennison, C. J. Hill, P. Vukusic, S. Doak, S. J. Martin, M. Hutchings, S. R. Parnell, C. Vasilev, N. Clarke, A. J. Ryan, W. Furnass, M. Croucher, R. M. Dalgliesh, S. Prevost, R. Dattani, A. Parker, R. A. L. Jones, J. P. A. Fairclough, A. J. Parnell, *Commun. Chem.* **2019**, 2, 100.
- [12] B. D. Wilts, X. Sheng, M. Holler, A. Diaz, M. Guizar-Sicairos, J. Raabe, R. Hoppe, S.-H. Liu, R. Langford, O. D. Onelli, D. Chen, S. Torquato, U. Steiner, C. G. Schroer, S. Vignolini, A. Sepe, *Adv. Mater.* **2018**, 30, 1702057.
- [13] D. T. Meiers, M. C. Heep, G. von Freymann, *APL Photonics* **2018**, 3, 100802.
- [14] L. Cortese, L. Pattelli, F. Utel, S. Vignolini, M. Burrelli, D. S. Wiersma, *Adv. Opt. Mater.* **2015**, 3, 1337.
- [15] S. M. Luke, B. T. Hallam, P. Vukusic, *Appl. Opt.* **2010**, 49, 4246.
- [16] S. H. Lee, S. M. Han, S. E. Han, *Opt. Mater. Express* **2021**, 11, 1692.
- [17] S. H. Lee, S. M. Han, S. E. Han, *APL Photonics* **2020**, 5, 056103.
- [18] G. Jacucci, L. Schertel, Y. Zhang, H. Yang, S. Vignolini, *Adv. Mater.* **2020**, 33, 2001215.
- [19] F. Utel, L. Cortese, D. S. Wiersma, L. Pattelli, *Adv. Opt. Mater.* **2019**, 7, 1900043.
- [20] W. Zou, L. Pattelli, J. Guo, S. Yang, M. Yang, N. Zhao, J. Xu, D. S. Wiersma, *Adv. Funct. Mater.* **2019**, 29, 1808885.
- [21] J. Syurik, G. Jacucci, O. D. Onelli, H. Hölscher, S. Vignolini, *Adv. Funct. Mater.* **2018**, 28, 1706901.
- [22] N. N. Shi, C.-C. Tsai, F. Camino, G. D. Bernard, N. Yu, R. Wehner, *Science* **2015**, 349, 298.
- [23] D. Ge, G. Wu, L. Yang, H.-N. Kim, W. Hallwachs, J. M. Burns, D. H. Janzen, S. Yang, *Proc. Natl. Acad. Sci. USA* **2017**, 114, 7379.
- [24] X. Liu, D. Wang, Z. Yang, H. Zhou, Q. Zhao, T. Fan, *Adv. Opt. Mater.* **2019**, 7, 1900687.
- [25] A. Dolinko, L. Borgmann, C. Lutz, E. R. Curticean, I. Wacker, M. S. Vidal, C. Szischik, Y. Donie, M. Inchaussandague, D. Skigin, H. Hölscher, P. Tubaro, A. Barreira, *Sci. Rep.* **2021**, 11, 19341.
- [26] D. Xie, Z. Yang, X. Liu, S. Cui, H. Zhou, T. Fan, *Soft Mater.* **2019**, 15, 4294.
- [27] C. Ye, M. Li, J. Hu, Q. Cheng, L. Jiang, Y. Song, *Environ. Sci.* **2011**, 4, 3364.
- [28] S. Yu, J. Chen, G. Liang, X. Ding, Y. Tang, Z. Li, *Bioinspir. Biomim.* **2020**, 15, 016003.
- [29] C.-C. Tsai, R. A. Childers, N. N. Shi, C. Ren, J. N. Pelaez, G. D. Bernard, N. E. Pierce, N. Yu, *Nat. Commun.* **2020**, 11, 551.
- [30] C. Lou, S. An, R. Yang, H. Zhu, Q. Shen, M. Jiang, B. Fu, P. Tao, C. Song, T. Deng, W. Shang, *APL Photonics* **2021**, 6, 036101.
- [31] M. Rothhammer, C. Zollfrank, K. Busch, G. von Freymann, *Adv. Opt. Mater.* **2021**, 9, 2100787.
- [32] R. Xiong, J. Luan, S. Kang, C. Ye, S. Singamaneni, V. V. Tsukruk, *Chem. Soc. Rev.* **2020**, 49, 983.
- [33] B. Yu, Z. Huang, D. Fang, S. Yu, T. Fu, Y. Tang, Z. Li, *Adv. Mater. Interfaces* **2022**, 9, 2101485.
- [34] T.-W. Koh, J. A. Spechler, K. M. Lee, C. B. Arnold, B. P. Rand, *ACS Photonics* **2015**, 2, 1366.
- [35] S. Yu, B. Fritz, S. Johnsen, D. Busko, B. S. Richards, M. Hippler, G. Wiegand, Y. Tang, Z. Li, U. Lemmer, H. Hölscher, G. Gomard, *Adv. Opt. Mater.* **2019**, 7, 1900223.
- [36] S. Yu, B. Guo, S. Johnsen, G. Wiegand, U. Lemmer, X. Guo, M. Zhang, Y. Li, C. Sprau, H. Hölscher, A. Colmann, G. Gomard, *Energy Technol.* **2022**, 10, 2100676.
- [37] J. Mandal, Y. Fu, A. C. Overvig, M. Jia, K. Sun, N. N. Shi, H. Zhou, X. Xiao, N. Yu, Y. Yang, *Science* **2018**, 362, 315.
- [38] P.-C. Hsu, A. Y. Song, P. B. Catrysse, C. Liu, Y. Peng, J. Xie, S. Fan, Y. Cui, *Science* **2016**, 353, 1019.
- [39] J. E. Mark, *Physical Properties of Polymers Handbook*, Springer, New York **2007**.
- [40] R. S. Stein, M. B. Rhodes, *J. Appl. Phys.* **1960**, 31, 1873.
- [41] G. Beadie, M. Brindza, R. A. Flynn, A. Rosenberg, J. S. Shirk, *Appl. Opt.* **2015**, 54, F139.
- [42] Z. Wang, C. L. C. Chan, T. H. Zhao, R. M. Parker, S. Vignolini, *Adv. Opt. Mater.* **2021**, 9, 2100519.
- [43] B. Frka-Petesic, S. Vignolini, *Nat. Photonics* **2019**, 13, 365.
- [44] M. S. Toivonen, O. D. Onelli, G. Jacucci, V. Lovikka, O. J. Rojas, O. Ikkala, S. Vignolini, *Adv. Mater.* **2018**, 30, 1704050.
- [45] M. Nogi, S. Iwamoto, A. N. Nakagaito, H. Yano, *Adv. Mater.* **2009**, 21, 1595.
- [46] H. Zhu, S. Parvianian, C. Preston, O. Vaaland, Z. Ruan, L. Hu, *Nanoscale* **2013**, 5, 3787.
- [47] Z. Fang, H. Zhu, Y. Yuan, D. Ha, S. Zhu, C. Preston, Q. Chen, Y. Li, X. Han, S. Lee, G. Chen, T. Li, J. Munday, J. Huang, L. Hu, *Nano Lett.* **2014**, 14, 765.
- [48] G. Hou, Y. Liu, D. Zhang, G. Li, H. Xie, Z. Fang, *ACS Appl. Mater. Interfaces* **2020**, 12, 31998.

- [49] Q.-F. Guan, K.-P. Yang, Z.-M. Han, H.-B. Yang, Z.-C. Ling, C.-H. Yin, S.-H. Yu, *ACS Mater. Lett.* **2021**, *4*, 87.
- [50] S. H. Choi, S.-W. Kim, Z. Ku, M. A. Visbal-Onufrak, S.-R. Kim, K.-H. Choi, H. Ko, W. Choi, A. M. Urbas, T.-W. Goo, Y. L. Kim, *Nat. Commun.* **2018**, *9*, 452.
- [51] B. K. Park, I. C. Um, S. M. Han, S. E. Han, *Adv. Photonics Res.* **2021**, *2*, 2100008.
- [52] J. Sarver, E. Kiran, *J. Supercrit. Fluids* **2021**, *73*, 105166.
- [53] C. M. Stafford, T. P. Russell, T. J. McCarthy, *Macromolecules* **1999**, *32*, 7610.
- [54] S. Yu, J. Yu, J. Chen, X. Ding, J. Li, L. Rao, Y. Tang, Z. Li, *Appl. Opt.* **2020**, *59*, 4533.
- [55] G.-L. Ni, X. Zhu, H.-Y. Mi, P.-Y. Feng, J. Li, X. Jing, B. Dong, C. Liu, C. Shen, *Nano Energy* **2021**, *87*, 106148.
- [56] D.-M. Wang, J.-Y. Lai, *Curr. Opin. Chem. Eng.* **2013**, *2*, 229.
- [57] Y. Tang, K. Wu, S. Yu, J. Chen, X. Ding, L. Rao, Z. Li, *Opt. Lett.* **2020**, *45*, 2918.
- [58] Y. J. Donie, M. Smeets, A. Egel, F. Lentz, J. B. Preinfalk, A. Mertens, V. Smirnov, U. Lemmer, K. Bittkau, G. Gomard, *Nanoscale* **2018**, *10*, 6651.
- [59] P. A. Levkin, F. Svec, J. M. Fréchet, *Adv. Funct. Mater.* **2009**, *19*, 1993.
- [60] F. Svec, J. M. Fréchet, *Chem. Mater.* **1995**, *7*, 707.
- [61] G. Liang, S. Yu, Z. Huang, K. Wu, T. Fu, Y. Tang, Z. Li, *Adv. Photonics Res.* **2021**, *2*, 2100185.
- [62] L. Xue, J. Zhang, Y. Han, *Prog. Polym. Sci.* **2012**, *37*, 564.
- [63] S. Walheim, E. Schäffer, J. Mlynek, U. Steiner, *Science* **1999**, *283*, 520.
- [64] Y. J. Donie, D. Theobald, S. Moghadamzadeh, A. Mertens, I. M. Hossain, U. W. Paetzold, U. Lemmer, G. Gomard, *Adv. Opt. Mater.* **2021**, *9*, 2001610.
- [65] Y. J. Donie, Y. Yuan, I. Allegro, F. Schackmar, I. M. Hossain, R. Huber, J. Roger, U. W. Paetzold, G. Gomard, U. Lemmer, *Adv. Mater. Technol.* **2021**, *7*, 2101008.
- [66] J. Yip, S.-P. Ng, K. Wong, *Text. Res. J.* **2009**, *79*, 771.
- [67] F. Zeighami, M. A. Tehran, *J. Ind. Text.* **2015**, *46*, 495.
- [68] Y. Tang, Z. Li, G. Liang, Z. Li, J. Li, B. Yu, *Opt. Express* **2018**, *26*, 27716.
- [69] Y. Tang, G. Liang, J. Chen, S. Yu, Z. Li, L. Rao, B. Yu, *Opt. Express* **2017**, *25*, 20598.
- [70] H. Zhong, Y. Li, P. Zhang, S. Gao, B. Liu, Y. Wang, T. Meng, Y. Zhou, H. Hou, C. Xue, Y. Zhao, Z. Wang, *ACS Nano* **2021**, *15*, 10076.
- [71] W. Jing, S. Zhang, W. Zhang, Z. Chen, C. Zhang, D. Wu, Y. Gao, H. Zhu, *ACS Appl. Mater. Interfaces* **2021**, *13*, 29558.
- [72] D. Li, X. Liu, W. Li, Z. Lin, B. Zhu, Z. Li, J. Li, B. Li, S. Fan, J. Xie, J. Zhu, *Nat. Nanotechnol.* **2021**, *16*, 153.
- [73] R. A. Yalçın, E. Blandre, K. Joulain, J. Drévilion, *Sol. Energy Mater. Sol. Cells* **2020**, *206*, 110320.
- [74] H. Kim, S. McSherry, B. Brown, A. Lenert, *ACS Appl. Mater. Interfaces* **2020**, *12*, 43553.
- [75] B. K. Park, S. M. Han, S. E. Han, *Opt. Mater. Express* **2022**, *12*, 2529.
- [76] H. J. Lee, S. An, J. H. Hwang, S.-G. Jung, H. S. Jo, K. N. Kim, Y. S. Shim, C. H. Park, S. S. Yoon, Y. W. Park, *ACS Appl. Mater. Interfaces* **2014**, *7*, 68.
- [77] Y. Tang, G. Liang, C. Song, Z. Li, S. Yu, X. Ding, *Mater. Lett.* **2018**, *227*, 104.
- [78] G. Liang, Y. Tang, P. Chen, J. Li, Y. Yuan, S. Yu, L. Xu, Z. Li, *ACS Appl. Polym. Mater.* **2021**, *4*, 91.
- [79] D. Wu, F. Xu, B. Sun, R. Fu, H. He, K. Matyjaszewski, *Chem. Rev.* **2012**, *112*, 3959.
- [80] S. Caixeiro, M. Peruzzo, O. D. Onelli, S. Vignolini, R. Sapienza, *ACS Appl. Mater. Interfaces* **2017**, *9*, 7885.
- [81] L. Zhou, J. Rada, H. Zhang, H. Song, S. Mirniaharikandi, B. S. Ooi, Q. Gan, *Adv. Sci.* **2021**, *8*, 2102502.
- [82] Y. Weng, W. Zhang, Y. Jiang, W. Zhao, Y. Deng, *Sol. Energy Mater. Sol. Cells* **2021**, *230*, 111205.
- [83] L. Zhou, J. Zhao, H. Huang, F. Nan, G. Zhou, Q. Ou, *ACS Photonics* **2021**, *8*, 3301.
- [84] A. Zhang, H. Bai, L. Li, *Chem. Rev.* **2015**, *115*, 9801.
- [85] A. Bertrand, F. Dumur, M. Mruczkiewicz, M. Perrin, C. Lartigau-Dagron, A. Bousquet, L. Vignau, L. Billon, S. Fasquel, *Org. Electron.* **2018**, *52*, 222.
- [86] Y. Peng, X. Guo, R. Liang, Y. Mou, H. Cheng, M. Chen, S. Liu, *ACS Photonics* **2017**, *4*, 2479.
- [87] F. Mayer, D. Ryklin, I. Wacker, R. Curticean, M. Čalkovský, A. Niemeyer, Z. Dong, P. A. Levkin, D. Gerthsen, R. R. Schröder, M. Wegener, *Adv. Mater.* **2020**, *32*, 2002044.
- [88] Y. J. Donie, S. Schliske, R. H. Siddique, A. Mertens, V. Narasimhan, F. Schackmar, M. Pietsch, I. M. Hossain, G. Hernandez-Sosa, U. Lemmer, G. Gomard, *ACS Nano* **2021**, *15*, 7305.
- [89] D. Lei, Y. Yang, Z. Liu, S. Chen, B. Song, A. Shen, B. Yang, S. Li, Z. Yuan, Q. Qi, L. Sun, Y. Guo, H. Zuo, S. Huang, Q. Yang, X. Mo, C. He, B. Zhu, E. M. Jeffries, F.-L. Qing, X. Ye, Q. Zhao, Z. You, *Mater. Horiz.* **2019**, *6*, 394.
- [90] F. Mayoussi, E. H. Doeven, A. Kick, A. Goralczyk, Y. Thomann, P. Risch, R. M. Guijt, F. Kotz, D. Helmer, B. E. Rapp, *J. Mater. Chem. A* **2021**, *9*, 21379.
- [91] Z. Dong, M. Vuckovac, W. Cui, Q. Zhou, R. H. A. Ras, P. A. Levkin, *Adv. Mater.* **2021**, *33*, 2106068.
- [92] Z. Dong, H. Cui, H. Zhang, F. Wang, X. Zhan, F. Mayer, B. Nestler, M. Wegener, P. A. Levkin, *Nat. Commun.* **2021**, *12*, 247.
- [93] S. Yu, Z. Li, G. Liang, Y. Tang, B. Yu, K. Chen, *Photonics Res.* **2016**, *4*, 140.
- [94] S. Yu, Y. Tang, Z. Li, K. Chen, X. Ding, B. Yu, *Photonics Res.* **2018**, *6*, 90.
- [95] X. Ding, C. Shao, S. Yu, B. Yu, Z. Li, Y. Tang, *Photonics* **2020**, *7*, 126.
- [96] G. Liang, S. Yu, Y. Tang, Z. Lu, Y. Yuan, Z. Li, J. Li, *IEEE Trans. Electron Devices* **2020**, *67*, 4530.
- [97] H. Go, T.-W. Koh, H. Jung, C. Y. Park, T.-W. Ha, E. M. Kim, M. H. Kang, Y. H. Kim, C. Yun, *Org. Electron.* **2017**, *47*, 117.
- [98] H. Go, E.-M. Han, M. H. Kang, Y. H. Kim, C. Yun, *Org. Electron.* **2019**, *67*, 79.
- [99] S. Yu, B. Zhuang, J. Chen, Z. Li, L. Rao, B. Yu, Y. Tang, *Opt. Lett.* **2017**, *42*, 4962.
- [100] M. Yu, M. H. Saeed, S. Zhang, H. Wei, Y. Gao, C. Zou, L. Zhang, H. Yang, *Adv. Funct. Mater.* **2021**, *32*, 2109472.
- [101] D. Theobald, S. Yu, G. Gomard, U. Lemmer, *ACS Photonics* **2020**, *7*, 1452.
- [102] G. Y. Kim, S. Kim, J. Choi, M. Kim, H. Lim, T. W. Nam, W. Choi, E. N. Cho, H. J. Han, C. Lee, J. C. Kim, H. Y. Jeong, S.-Y. Choi, M. S. Jang, D. Y. Jeon, Y. S. Jung, *Nano Lett.* **2019**, *19*, 6827.
- [103] A. P. Raman, M. A. Anoma, L. Zhu, E. Rephaeli, S. Fan, *Nature* **2014**, *515*, 540.
- [104] T. Li, Y. Zhai, S. He, W. Gan, Z. Wei, M. Heidarinejad, D. Dalgo, R. Mi, X. Zhao, J. Song, J. Dai, C. Chen, A. Aili, A. Vellore, A. Martini, R. Yang, J. Srebric, X. Yin, L. Hu, *Science* **2019**, *364*, 760.
- [105] T. Wang, Y. Wu, L. Shi, X. Hu, M. Chen, L. Wu, *Nat. Commun.* **2021**, *12*, 365.
- [106] J. Wu, J. He, K. Yin, Z. Zhu, S. Xiao, Z. Wu, J.-A. Duan, *Nano Lett.* **2021**, *21*, 4209.
- [107] H. Zhao, Q. Sun, J. Zhou, X. Deng, J. Cui, *Adv. Mater.* **2020**, *32*, 2000870.
- [108] A. Leroy, B. Bhatia, C. C. Kelsall, A. Castillejo-Cuberos, M. H. Di Capua, L. Zhao, L. Zhang, A. M. Guzman, E. N. Wang, *Sci. Adv.* **2019**, *5*, eaat9480.
- [109] M. Yang, W. Zou, J. Guo, Z. Qian, H. Luo, S. Yang, N. Zhao, L. Pattelli, J. Xu, D. S. Wiersma, *ACS Appl. Mater. Interfaces* **2020**, *12*, 25286.
- [110] Y. Peng, J. Chen, A. Y. Song, P. B. Catrysse, P.-C. Hsu, L. Cai, B. Liu, Y. Zhu, G. Zhou, D. S. Wu, *Nat. Sustain.* **2018**, *1*, 105.

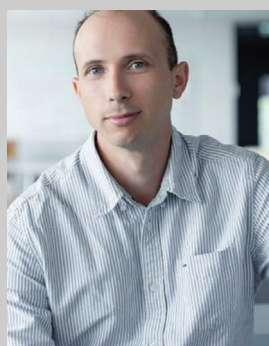
- [111] A. Yang, L. Cai, R. Zhang, J. Wang, P.-C. Hsu, H. Wang, G. Zhou, J. Xu, Y. Cui, *Nano Lett.* **2017**, *17*, 3506.
- [112] S. Zeng, S. Pian, M. Su, Z. Wang, M. Wu, X. Liu, M. Chen, Y. Xi-ang, J. Wu, M. Zhang, Q. Cen, Y. Tang, X. Zhou, Z. Huang, R. Wang, A. Tunuhe, X. Sun, Z. Xia, M. Tian, M. Chen, X. Ma, L. Yang, J. Zhou, H. Zhou, Q. Yang, X. Li, Y. Ma, G. Tao, *Science* **2021**, *373*, 692.
- [113] J. Chen, S. Yu, T. Fu, L. Xu, Y. Tang, Z. Li, *Bioinspir. Biomim.* **2022**, *17*, 026007.
- [114] Y. Peng, Y. Cui, *Joule* **2020**, *4*, 724.
- [115] P. Tao, G. Ni, C. Song, W. Shang, J. Wu, J. Zhu, G. Chen, T. Deng, *Nat. Energy* **2018**, *3*, 1031.
- [116] F. Zhao, Y. Guo, X. Zhou, W. Shi, G. Yu, *Nat. Rev. Mater.* **2020**, *5*, 388.
- [117] D. E. McCoy, A. V. Shneidman, A. L. Davis, J. Aizenberg, *Micron* **2021**, *151*, 103160.
- [118] M. Chen, D. Pang, J. Mandal, X. Chen, H. Yan, Y. He, N. Yu, Y. Yang, *Nano Lett.* **2021**, *21*, 1412.
- [119] D. Theobald, D. Beutel, L. Borgmann, H. Mescher, G. Gomard, C. Rockstuhl, U. Lemmer, J. *Quant. Spectrosc. Radiat. Transfer* **2021**, *272*, 107802.



Shudong Yu received his B.S. degree in 2014 and Ph.D. degree in 2019 from South China University of Technology (SCUT). After working as a postdoc at SCUT and The Hong Kong Polytechnic University for three years, he joined the School of Advanced Manufacturing, Sun Yat-sen University as an Assistant Professor in 2023. His research interests include light management for optoelectronics, biomimetics, solar energy.



Junchi Chen is currently a Ph.D. student at Light Technology Institute (LTI), Karlsruhe Institute of Technology (KIT). He received his Bachelor's degree in 2017 and his Master's degree in 2019 from South China University of Technology (SCUT). His research focuses on the light management and the color conversion of quantum dot materials.



Guillaume Gomard holds a Ph.D. degree in Materials Science from the École Centrale de Lyon (France) for his work on photonic crystals applied to photovoltaics. Between 2013 and 2020, he led the “Nanophotonics” research group at the Karlsruhe Institute of Technology (Germany). His research focused on the simulation and fabrication of disordered and bio-inspired optical materials, including light scattering porous media, as well as, their application for optoelectronic devices. Since 2020, he is working as a Senior Scientist at the company Carl Zeiss AG, where he develops imaging and spectroscopic-based solutions in the field of precision farming.



Hendrik Hölscher is head of the Biomimetics Group at the Institute of Microstructure Technology (IMT) at Karlsruhe Institute of Technology (KIT) since 2008. His research focusses on bio-inspired smart surfaces. He studied Physics and obtained his Ph.D. in 1999 at the University of Hamburg. Concentrating on the development of advanced atomic force microscopy techniques he worked for different research institutes before he established his own research group at the Center for NanoTechnology (CeNTech) of the University of Münster, Germany, in 2003. From 2006 to 2007 he stayed at the Department of Mechanical Engineering at Yale University as Visiting Assistant Professor.



Uli Lemmer received the Diploma degree from RWTH Aachen University in 1990 and a Ph.D. from the University of Marburg in 1995. He then held a postdoctoral position with the University of California at Santa Barbara. Afterward, he was heading the Organic Optoelectronics group at the University of Munich from 1996 to 2002. In 2002 he was appointed a Full Professor of Electrical Engineering and Information Technology and Director of the Light Technology Institute, Karlsruhe Institute of Technology (KIT). His research interests are in the field of optoelectronics and the technology and the applications of printable organic and inorganic materials.